# Mechanisms for Thermal Conduction in Methane Hydrate

Niall J. English*

*The SEC Strategic Research Cluster and the Centre for Synthesis and Chemical Biology, School of Chemical and Bioprocess Engineering, Conway Institute of Biomolecular and Biomedical Research, University College Dublin, Belfield, Dublin 4, Ireland*

John S. Tse†

*Department of Physics and Engineering Physics, University of Saskatchewan, Saskatoon, Saskatchewan S7N 5E2, Canada*

(Received 25 February 2009; published 30 June 2009)

Crystalline clathrate hydrates exhibit an unusual thermal transport with glasslike thermal conductivity close to the Debye temperature but a crystal-like temperature dependence at low temperature. Molecular dynamics calculations on structure I methane clathrate hydrate reproduced the qualitative trend in the thermal conductivity. Analysis of the heat flux and local energy correlation functions shows that both the crystal structure of the clathrate framework and guest-host interactions contribute to thermal transport processes. The lower thermal conductivity relative to ice *Ih* is due to differences in crystal structures. The glasslike temperature dependence is governed by the guests and the guest-host interactions.

DOI: 10.1103/PhysRevLett.103.015901 PACS numbers: 65.40.−b, 63.20.Ry, 64.70.kt

Methane hydrate is a nonstoichiometric inclusion compound with water forming a crystalline framework encaging methane molecules [1]. Its most peculiar property is a very low thermal conductivity compared to ice. Above 100 K (ca. Debye temperature $\Theta_D$ of 226 K [2]), its thermal conductivity displays a weak temperature dependence, resembling amorphous solids [3,4]. At lower temperatures, however, recent experiments show the temperature dependence of the clathrate's thermal conductivity is reversed [5,6]. Instead of decreasing monotonously with temperature, the thermal conductivity profile shows several distinct features, not unlike a crystal. Similar behavior has also been observed in some semiconductor clathrates [7–9]. This anomalous ''glasslike'' behavior at higher temperatures has been exploited by the principle of phonon glass electron crystals [9,10] for the engineering of new efficient thermoelectric materials.

Currently there is no conclusive explanation on this unusual thermal transport phenomenon. Several hypotheses have been suggested. The most studied being the ''resonant scattering'' model [4,11–14]. It is suggested energy transfer [11] between rattling motions of the guests with the lattice acoustic phonons is the cause for the dissipation of the thermal transport. This model provides a plausible mechanism for the dissipation of heat energy carried by the guests is through their rattling motion. A consequence of this model is that phonon scattering will be relatively inefficient if the temperature (thermal energy) is lower than the rattling vibrations. This conjecture is apparently supported by experiments on methane [5] and Xe [6] hydrates. In methane hydrate, glasslike thermal conductivity is no longer observed at temperatures below 90 K (i.e., 60 $cm^{-1}$ energy) but increases with decreasing temperature reaching a maximum at 40 K as in a crystal [5]. However, two recent experimental studies [15,16] on skutterides resulted in conflicting conclusions on this mechanism [17]. A fundamental understanding of transport mechanism in methane hydrate is relevant to the rationalization of the thermal behavior in related silicon clathrates and skutterudites [15,16].

Classical molecular dynamics (MD) simulations were performed on the prototypical structure I (SI) methane hydrate (MH), a hypothetical empty hydrate (EH), and ice *Ih*, since their properties are closely related. Earlier the low thermal conductivity of clathrate hydrates was attributed to the large unit cell [18]. Therefore, studies of all three systems are needed to delineate different contributing factors to the thermal conductivity in clathrate hydrates. Comparison of the results between empty clathrate and ice provides information on the contribution of crystal structures to thermal transport. A comparison of thermal conductivity behavior of empty and filled clathrates provides directly information on the role of the guests. Thermal conductivity was calculated from Green-Kubo (GK) linear response theory [19] via the heat flux autocorrelation function (HCACF) using equilibrium MD. This method has been applied to Xe [20] and methane hydrates [21–23] and metallic germanium clathrate [24]. Nonequilibrium MD [20,23] have also been used to predict thermal conductivity of methane hydrate. However, only recently, it was recognized that truncations of long-range electrostatic interactions in charged systems lead to errors in the stress tensor [25,26]. This shortcoming may affect the HCACF markedly [25,27]. Here, conductivity calculations were performed on MH, EH, and ice *Ih* from 30 to 265 K using GK theory with the correct implementation of long-range electrostatics. The starting coordinates of the oxygen atoms in the model unit cells of SI hydrate [28] and ice *Ih* [29] were taken from x-ray diffraction data, using proton-disordered cells. The simulation methodology is

 

described in the supplementary material [30], with production MD simulations on configurations relaxed at 30, 100, 150, 200, and 220 K (ice), and, in addition, 265 K (SI hydrate) and 1 bar. The ice and hydrate structures were stable throughout the relaxation and production runs.

In the calculation of the heat flux vector $\mathbf{J}$ there is an interactive term which is a pairwise summation over the forces exerted by atomic sites on one another [31]. The species enthalpy correction term requires that the total enthalpy of the system is decomposed into contributions from each species (i.e., water and methane) [31]. Because of the partial transformation from pairwise, real-space treatment to a reciprocal space form in Ewald electrostatics, it is necessary to recast the diffusive and interactive terms in this expression in a form amenable for use with the Ewald method using the recent reformulation of Petravic [27]. The thermal conductivity [32] ($k = \frac{V}{3k_B T^2} \times \int_0^\infty \langle \mathbf{J}(t) \cdot \mathbf{J}(0) \rangle dt$) was evaluated from the HCACF using Romberg integration in conjunction with cubic spline interpolation [33]. The integration times of 100 ps at 30 K, 50 ps at 100 and 150 K, and 20 ps at 200 K and above, with a sampling ratio of 30:1 or higher, were more than sufficient to provide a reliable estimate of the thermal conductivity at each temperature.

The thermal conductivity-temperature profile of a crystalline solid is well known. Above $\Theta_D/2$, it exhibits a $T^{-1}$ dependence due to umklapp processes [34,35]. Then it increases as temperature decreases reaching a maximum near $\Theta_D/10$. In this regime, the measured conductivity is heavily dependent on defects. Below around $\Theta_D/10$, conductivity has $T^3$ dependence, governed mainly by boundary scatterings. The calculated MH conductivity [Fig. 1(b)] is found to converge within numerical accuracy for $3 \times 3 \times 3$ and $4 \times 4 \times 4$ supercells. At 265 K, the respective calculated conductivities of 0.64 and $0.65 \pm 0.05$ $\mathrm{Wm^{-1}\,K^{-1}}$ agree well with observed values [21,36] of 0.62–0.68 $\mathrm{Wm^{-1}\,K^{-1}}$. Although the calculated ice *Ih* conductivity at 220 K of $1.03 \pm 0.05$ $\mathrm{Wm^{-1}\,K^{-1}}$ is lower than observed value of 2.4 $\mathrm{Wm^{-1}\,K^{-1}}$ [37], it is consistent with a previous calculation [19]. Computed conductivities for MH, EH, and ice are compared in Fig. 1(b). The crystalline behavior expected for ice *Ih* and EH is predicted. However, the temperature profile for MH is different. From 265 to 150 K, the MH conductivity is *lower* than EH and decreases slightly with temperature. A minimum is predicted at 100–150 K, and then the conductivity increases with decreasing temperature. The observations are consistent with experimental results [5,6].

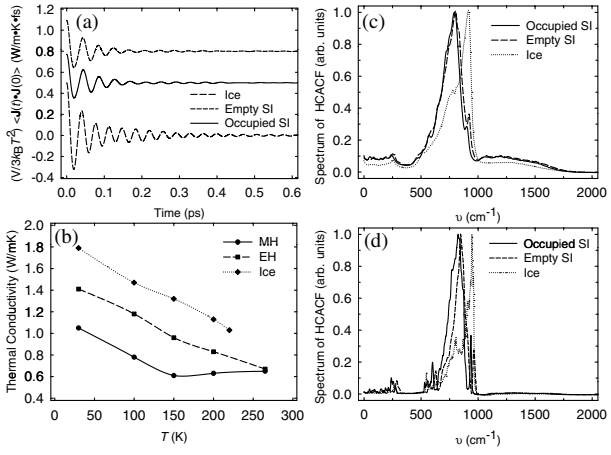


FIG. 1 (color online). (a) Normalized HCACF at 200 K for MH and EH and 220 K for ice. Those for MH and ice have been displaced upwards by 0.5 and 0.8, respectively, for clarity. (b) Temperature dependence of calculated thermal conductivity of MH and ice *Ih* with temperature. Real Fourier transform of normalized HCACF (arbitrary units) at (c) 200 K and (d) 30 K. Simulation boxes were composed of $3 \times 3 \times 3$ and $4 \times 4 \times 4$ unit cells of SI hydrate and $2 \times 2 \times 2$ fundamental ice *Ih* cells (transformed to orthorhombic structure from $5 \times 3 \times 3$ hexagonal unit cells) [28].

Relaxation times related to energy transfer times between neighboring atoms for phonon transport may be extracted by fitting HCACFs to sums of exponentially decaying functions [38–40]. These relaxation times are usually characterized by two time regimes—a rapid initial drop followed by a long decay [38].

$$\mathrm{HCACF}\,(t) = \sum_{i=1}^{n\_\mathrm{ac}} A_i \exp(-t/\tau_i) + \sum_{j=1}^{n\_\mathrm{opt}} \left( \sum_{k=1}^{n\_o,j} B_{jk} \exp(-t/\tau_{jk}) \right) \cos\omega_{0,j} t + \sum_{j=1}^{n\_\mathrm{opt}} C_j \cos\omega_{0,j} t. \quad (1)$$

The fitting procedure is described in the supplementary material [30]. HCACFs for ice, MH, and EH at 200–220 K are shown in Fig. 1(a). Oscillatory features arise from localized optic modes [40] ($\omega_0$), as confirmed by Fourier transformation [power spectra in Figs. 1(c) and 1(d)]. A peak in the power spectrum does not indicate that vibrational mode's involvement in heat transport. Contrarily, it reflects the localized nature of an isolated harmonic oscillator. In Fig. 1(c), at high temperature, the low frequency region below 300 $\mathrm{cm^{-1}}$ in MH's power spectra is featureless, indicating substantial coupling of water translations with guest vibrations in thermal transport. Distinctive features were observed at lower temperatures, again suggesting that these vibrations are more harmonic and dissipate less heat. Results of fits to ice, MH, and EH data are summarized in Table I for two temperatures. For ice and EH, the two-term fits (short- and long-range acoustic, $\tau_{\mathrm{sh,ac}}$ and $\tau_{\mathrm{lg,ac}}$) are adequate. For MH above 100 K, an additional medium-range relaxation time ($\tau_{\mathrm{int,ac}}$) is needed to achieve an optimal fit. The long-range $\tau_{\mathrm{lg,ac}}$, responsible for the bulk of heat transport generally decreases with increasing temperature, but those of MH and EH are broadly similar and lower than in ice. In MH, the unique $\tau_{\mathrm{int,ac}}$ is between $\tau_{\mathrm{sh,ac}}$ and $\tau_{\mathrm{lg,ac}}$ and is relatively insensitive

TABLE I. Acoustic relaxation times and contributions to the overall thermal conductivity based on fitting procedure, in $\mathrm{Wm^{-1}\,K^{-1}}$, for SI MH, EH, and ice *Ih* at two selected temperatures.

| Type | $T$ (K) | $\tau_{\mathrm{sh,ac}}$ (ps) | Short-range acoustic | $\tau_{\mathrm{int,ac}}$ (ps) | Medium-range acoustic | $\tau_{\mathrm{lg,ac}}$ (ps) | Long-range acoustic | Optic | Total |
|---|---|---|---|---|---|---|---|---|---|
| SI | 30 | $0.38 \pm 0.062$ | 0.21 | | | $4.4 \pm 0.39$ | 0.69 | 0.15 | $1.05 \pm 0.06$ |
| | 265 | $0.046 \pm 0.005$ | 0.06 | $0.33 \pm 0.16$ | 0.05 | $2.1 \pm 0.27$ | 0.40 | 0.13 | $0.64 \pm 0.05$ |
| Empty SI | 30 | $0.44 \pm 0.056$ | 0.20 | | | $6.1 \pm 0.49$ | 0.99 | 0.22 | $1.41 \pm 0.06$ |
| | 265 | $0.057 \pm 0.0047$ | 0.08 | | | $2.2 \pm 0.23$ | 0.43 | 0.16 | $0.67 \pm 0.05$ |
| Ice | 30 | $0.47 \pm 0.068$ | 0.24 | | | $8.2 \pm 0.58$ | 1.31 | 0.24 | $1.79 \pm 0.08$ |
| | 220 | $0.23 \pm 0.034$ | 0.11 | | | $2.4 \pm 0.23$ | 0.72 | 0.20 | $1.03 \pm 0.07$ |

to temperature (~0.3–0.4 ps). The medium relaxation time of 0.2–0.4 ps is consistent with an effective guest-water relaxation time of ~0.1 ps obtained from the analysis of tetrahydrofuran hydrate conductivity with the resonant scattering model [4] and the calculated lifetimes of strongly scattered phonon modes in Xe hydrate [12] of 0.3–1.0 ps. The high frequency (optic) HCACF decay components are modulated by cosine functions [Eq. (1)] with characteristic frequencies extracted from power spectra [Figs. 1(c) and 1(d)]. Calculated contributions are summarized in Table I, the largest being from the long-range acoustic term. In MH, the short- and intermediate-range acoustic terms contribute equally. In EH, short-range acoustic and optic contributions are almost equal. For ice at 220 K, the optic contribution of 0.13 $\mathrm{Wm^{-1}\,K^{-1}}$, which accounts for 13% of the total conductivity, is in excellent agreement with ca. 10% estimated from high quality experimental data [37].

To probe the heat transfer through guest-host interactions, energy correlation functions (ECFs) were computed [38,39]. ECF is the deviation of the water-methane interaction energy from its long-time average value: $\mathrm{ECF_{WM}}(t) = \langle \Delta U_{\mathrm{WM}}(t) \Delta U_{\mathrm{WM}}(0) \rangle / \langle \Delta U_{\mathrm{WM}}(0) \Delta U_{\mathrm{WM}}(0) \rangle$ and $\Delta U_{\mathrm{WM}}(t) = U_{\mathrm{WM}}(t) - \langle U_{\mathrm{WM}}(t) \rangle$ are calculated from 30 to 265 K and shown in Fig. 2(a). Damping is visible clearly at and above 150 K. Below 150 K, the ECF of the methane-water interaction energy is almost harmonic with no damping indicating heat dissipation is small. This agrees with the experimental observation that conductivity starts to increase at 90 K. Above 150 K, strong ECF damping was observed. Moreover, a short oscillation period of 0.14 ps was identified, which may be related to short acoustic relaxation ($2\tau_{\mathrm{sh,ac}}$). To characterize guest-host interactions further, the MH heat flux vector $\mathbf{J}$ is decomposed into contributions arising from water and methane molecules, i.e., $\mathbf{J} = \mathbf{J}_w + \mathbf{J}_m$. The sum of the integral of the separate components is essentially identical to the overall HCACF. It was found that thermal conductivity through water in MH was less than that of EH. Furthermore, methane and methane-water terms contribute more at higher temperatures, with combined percentages increasing steadily from 3%–8% between 30 and 200 K, confirming the unique role of methane in clathrate thermal conductivity. $\mathbf{J}_{\mathrm{W}}$ ACF fits for short- and long-range acoustic times are very close to those of the MH full HCACF. Conversely, the $\mathbf{J}_{\mathrm{W}}\mathbf{J}_{\mathrm{M}}$ cross correlation function (CCF) has a single relaxation time near the full HCACF's intermediate range $\tau_{\mathrm{int,ac}}$ at 150–265 K (~0.3–0.4 ps; cf. Table I), suggesting that the medium-range relaxation above 100 K arises from water-methane interactions. The increasing importance and decreasing relaxation times of $\mathbf{J}_{\mathrm{W}}\mathbf{J}_{\mathrm{M}}$ CCF and $\mathbf{J}_{\mathrm{M}}$ ACF with increasing temperature is, again,

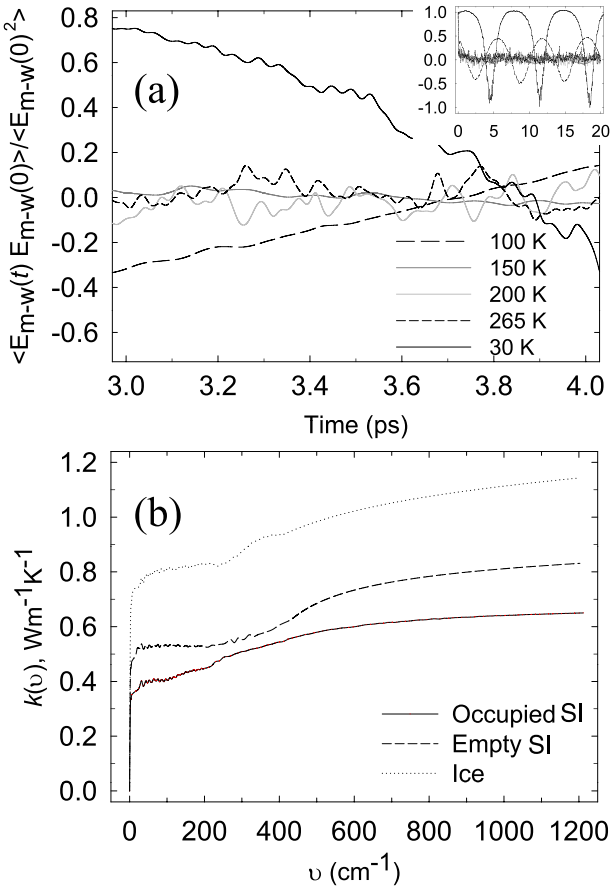


FIG. 2 (color online). (a) Normalized ACF of methane-water interaction energies in SI MH at various temperatures at a time slice of 1 ps (3–4 ps); (inset) the full 20 ps ACF. (b) Thermal conductivity evaluated from GK integral of reverse-transformed low bandpass filtered HCACF at each given frequency [$K(\omega)$] at 200 K. The arrows signify the three distinct regions (see text).

an indication of stronger and faster heat dissipation via gust-host interactions.

The cumulative frequency thermal conductivity [39] $K(\omega)$, obtained by integrating the inverse transformation of the filtered HCACF spectrum up to $\omega$, is shown in Fig. 2(b) for ice, MH, and EH and has three distinct regions. At low frequency, conductivity rises rapidly (I), followed by a relatively ''flat'' region (II), with steady rises into optical frequencies (III). It should be noted that frequencies in the GK approach are related to phonon-phonon interactions [39]. Region II, ca. 50–300 $cm^{-1}$, overlaps with translational vibrations, while region III's beginning coincides with the onset of host librations. The ice and EH profiles are quite similar, but differ from MH. In MH, no clear discontinuity was observed between regions II and III, and $K(\omega)$ increases gradually to higher frequencies, emphasizing intermediate relaxation.

In summary, classical MD calculations reproduced experimental thermal conductivities of ice, MH, and EH semiquantitatively. Significantly, the observed reversal in MH's temperature dependence at 90 K is predicted. Since the water-methane interaction is weak, scattering of thermal phonons is much more efficient at higher temperature (>100 K). Collisions of the guests with the water cages ''dephase'' the heat-carrying lattice acoustic phonons, resulting in the localization of energy and lower thermal conductivity. Calculations show EH's conductivity behavior is similar to ice, except with lower absolute values, due mainly to smaller long-range relaxation times $\tau_{lg,ac}$ (Table I) and shorter phonon mean free paths. A similar observation has been made in zeolites, with distortions of $SiO_4$ suggested as the cause [40]. In hydrates, the water hydrogen bond network [41] is more strained than in ice, this would result in inhibition of long-range modes and spatial localization of energy. This conjecture suggests that thermal conductivity depends not only on guest-host interactions, but is also related to rigidity of the framework. This helps to rationalize the apparent absence of ''resonant scattering'' in some semiconductor clathrates and skutterudites and the low conductivity in empty silicon clathrate [15–17]

*Niall.English@ucd.ie
†John.Tse@usask.ca

[1] D. E. Sloan and C. Koh *Clathrate Hydrates of Natural Gases* (CRC Press, Boca Raton, FL, 2007), 3rd ed.
[2] J. S. Tse, J. Phys. (Paris), Colloq. **48**, C1-543 (2007).
[3] R. G. Ross, P. Andersson, and G. Bäckström, Nature (London) **290**, 322 (1981).
[4] J. S. Tse and M. A. White, J. Phys. Chem. **92**, 5006 (1988).
[5] A. I. Krivchikov *et al.*, J. Low Temp. Phys. **139**, 693 (2005).
[6] A. I. Krivchikov *et al.*, Phys. Rev. B **73**, 064203 (2006).
[7] G. S. Nolas *et al.*, Appl. Phys. Lett. **82**, 910 (2003).
[8] J. L. Cohn *et al.*, Phys. Rev. Lett. **82**, 779 (1999).
[9] G. A. Slack, in *Thermoelectric Materials—New Directions and Approaches*, edited by T. M. Tritt, M. G. Kanatzidis, H. B. Lyon, and G. D. Mahan, MRS Symposia Proceedings No. 468 (Materials Research Society, Pittsburgh, 1997), p. 47.
[10] G. S. Nolas, D. T. Morelli, and T. M. Tritt, Annu. Rev. Mater. Sci. **29**, 89 (1999).
[11] J. S. Tse *et al.*, J. Phys. Chem. A **101**, 4491 (1997).
[12] J. S. Tse *et al.*, Europhys. Lett. **54**, 354 (2001).
[13] J. Baumert *et al.*, Phys. Rev. B **68**, 174301 (2003).
[14] J. S. Tse *et al.*, Nature Mater. **4**, 917 (2005).
[15] M. M. Koza *et al.*, Nature Mater. **7**, 805 (2008).
[16] M. Christensen *et al.*, Nature Mater. **7**, 811 (2008).
[17] C. B. Vining, Nature Mater. **7**, 765 (2008).
[18] M. W. C. Dharma-Wardana, J. Phys. Chem. **87**, 4185 (1983).
[19] D. A. McQuarrie, *Statistical Mechanics* (University Science Books, Herndon, VA, 2000).
[20] R. Inoue, H. Tanaka, and K. Nakanishi, J. Chem. Phys. **104**, 9569 (1996).
[21] E. J. Rosenbaum *et al.*, J. Phys. Chem. B **111**, 13 194 (2007).
[22] N. J. English, Mol. Phys. **106**, 1887 (2008).
[23] H. Jiang *et al.*, J. Phys. Chem. B **112**, 10 207 (2008).
[24] J. J. Dong, O. K. Sankey, and C. W. Myles, Phys. Rev. Lett. **86**, 2361 (2001).
[25] N. Galamba, C. A. Nieto de Castro, and J. F. Ely, J. Chem. Phys. **120**, 8676 (2004).
[26] N. Galamba, C. A. Nieto de Castro, and J. F. Ely, J. Phys. Chem. B **108**, 3658 (2004).
[27] J. Petravic, J. Chem. Phys. **123**, 174503 (2005).
[28] R. K. McMullan and G. A. Jeffrey, J. Chem. Phys. **42**, 2725 (1965).
[29] J. A. Hayward and J. R. Reimers, J. Chem. Phys. **106**, 1518 (1997).
[30] See EPAPS Document No. E-PRLTAO-103-064928 for computational details and procedures. For more information on EPAPS, see http://www.aip.org/pubservs/epaps.html.
[31] R. Vogelsang and C. Hoheisal, Phys. Rev. A **35**, 3487 (1987).
[32] D. J. Evans and G. P. Morriss, *Statistical Mechanics of Nonequilibrium Liquids* (Academic, San Diego, 1990).
[33] W. H. Press *et al.*, *Numerical Recipes* (Cambridge University Press, Cambridge, England, 1992), 2nd ed.
[34] T. M. Tritt, *Thermal Conductivity: Theory, Properties, and Applications* (Kluwer Academic, New York, 2004).
[35] A. J. H. McGaughey and M. Kaviany, Adv. Heat Transf. **39**, 169 (2006).
[36] W. F. Waite *et al.*, Geophys. J. Int. **169**, 767 (2007).
[37] G. A. Slack, Phys. Rev. B **22**, 3065 (1980).
[38] A. J. C. Ladd, W. Moran, and W. G. Hoover, Phys. Rev. B **34**, 5058 (1986).
[39] A. J. H. McGaughey and M. Kaviany, Int. J. Heat Mass Transf. **47**, 1783 (2004).
[40] A. J. H. McGaughey and M. Kaviany, Int. J. Heat Mass Transf. **47**, 1799 (2004).
[41] C. Gutt *et al.*, J. Chem. Phys. **113**, 4713 (2000).